DOE/ER/03077-266

Courant Mathematics and
Computing Laboratory

U.S. Department of Energy

Applications of Front Tracking to Combustion, Surface Instabilities and Two Dimensional Riemann Problems: A Conference Report

B. Bukiet, C. L. Gardner, J. Glimm,
J. Grove, J. Jones, O. McBryan,
R. Menikoff, and D. H. Sharp

Research and Development Report

Supported by the Applied Mathematical Sciences
subprogram of the Office of Energy Research,
U.S. Dept. of Energy under Contract DE-AC02-76ER03077

Mathematics and Computers

August 1985

NEW YORK UNIVERSITY

DOE/ER/03077-266
UC-32
Mathematics and Computers

APPLICATIONS OF FRONT TRACKING TO COMBUSTION, SURFACE INSTABILITIES AND TWO DIMENSIONAL RIEMANN PROBLEMS: A CONFERENCE REPORT

B. Bukiet*, C. L. Gardner*, J. Glimm*,
J. Grove*, J. Jones*, O. McBryan*,
R. Menikoff†, and D. H. Sharp†

August 1985

Supported by the Applied Mathematical Sciences subprogram of the Office of Energy Research, U. S. Department of Energy under Contract No. DE-AC02-76ER03077

* Courant Institute of Mathematical Sciences, New York University, New York, NY

† Los Alamos National Laboratory, Los Alamos, NM

Contents

DISCLAIMER

Printed in U.S.A.

Available from

National Technical Information Service
U.S. Department of Commerce
5285 Port Royal Road
Springfield, VA 22161

Applications of Front Tracking to Combustion, Surface Instabilities and Two Dimensional Riemann Problems: A Conference Report

Bruce Bukiet [5,6]
Carl L. Gardner [2]
James Glimm [1,2,3]
John Grove [3]
James Jones [5,6]
Oliver McBryan [1,2,6,7]

Courant Institute of Mathematics
New York University
New York, New York 10012

Ralph Menikoff [4]
David H. Sharp [4]

Los Alamos National Laboratory
Los Alamos, New Mexico 87545

ABSTRACT

The method of front tracking is applied to problems involving curved detonation fronts, surface instabilities and two-dimensional Riemann problems. The detonation problems include detonation fronts with and without cylindrical symmetry; comparisons with one-dimensional models are made. The analysis of interface instabilities focuses on the compressible Rayleigh-Taylor instability of a supersonic accelerated contact discontinuity between two gases and the propagation of a supersonic slab jet. Theoretical notions for an S matrix theory for general multi-dimensional hyperbolic conservation laws and the numerical implementation of computer programs which solve certain two-dimensional Riemann problems are also discussed.

1. Supported in part by the National Science Foundation, grant DMS-83-1229.
2. Supported in part by the Applied Mathematical Sciences subprogram of the Office of Energy Research, U. S. Department of Energy, under contract DE-AC02-76ER03077.
3. Supported in part by the Army Research Office, grant DAAG29-83-K-0007.
4. Work supported by the U. S. Department of Energy.
5. Supported in part by the National Science Foundation, grant nos. MCS-82-07965 and MCS-83-01662.
6. Supported in part by the Army Research Office, grant DAAG-29-84-K0130.
7. Alfred P. Sloan Foundation Fellow.

1. Introduction

Systems of non-linear conservation laws in n space dimensions

$$\mathbf{u}_t + \vec{\nabla}\cdot\vec{F}(\mathbf{x}, \mathbf{u}) = 0 \tag{1.1}$$

where $\mathbf{u} = \mathbf{u}(\mathbf{x}, t)$ and $\vec{F}$ is a smooth function of the state $\mathbf{u} \in R^s$ and the position $\mathbf{x} \in R^n$ into R^s, are often used as first order approximations for many natural phenomena. Equations of this type occur in models in which external forces and higher order effects such as viscosity and heat conduction are neglected.

We are primarily concerned with the case where system (1.1) consists of the Euler equations for a compressible, inviscid, non-heat conducting gas. In this case:

$$\mathbf{u} = \begin{pmatrix} \rho \\ \mathbf{m} \\ E \end{pmatrix} \text{ and } \vec{F}(\mathbf{u}) = \begin{pmatrix} \mathbf{m} \\ \dfrac{\mathbf{m}\otimes\mathbf{m}}{\rho} + p \\ \dfrac{\mathbf{m}}{\rho}(E+p) \end{pmatrix}. \tag{1.2}$$

Here ρ is the density, $\mathbf{m}$ and E are the momentum and total energy per unit volume respectively and p is the thermodynamic pressure. These equations represent the laws of conservation of mass, momentum and energy respectively. The thermodynamic variables p, ρ and E are related by a caloric equation of state $p = p(\rho, E)$. For the case of a polytropic gas this relation is given by:

$$p = (\gamma-1)\left[E - \frac{|\mathbf{m}|^2}{2\rho}\right],$$

where γ is positive constant usually satisfying $1<\gamma\leq\frac{5}{3}$.

Much progress has recently been made in adapting a front tracking method to the calculation of solutions of system (1.1) which contain discontinuities. In this method a one-dimensional grid is placed onto the discontinuity. Points on the tracked front are propagated by solving one-dimensional Riemann problems in the direction normal to the interface. This step provides the position of the tracked interface for the next time step. Tangential information is ignored during the normal propagation phase, so this step is followed by a update of the states on the new interface based on the component of (1.1) tangent to the interface. The

positions of the new and old fronts together with their assigned states are used as boundary value data for the solution of the states off the front. A detailed description of this method can be found in [1].

The discontinuities supported by the Euler equations (1.2) are of two types, shocks and contact discontinuities. If combustion is considered, a third type of discontinuity, a combustion wave, may also occur.

In this paper we will report on recent progress which has been made by the authors and co-workers in modeling solutions in two space dimensions of the Euler equations for detonation waves, surface instabilities for non-combustion interactions and the numerical solution of certain two-dimensional Riemann problems. In addition recent theoretical work concerning a general theory of elementary waves and Riemann solutions for systems of hyperbolic conservation laws will also be discussed.

2. Multi-dimensional Riemann Problems and Elementary Waves

While the theory of hyperbolic conservation laws in one space dimension is highly developed, the corresponding theory for two or more space dimensions is not so well understood. Recent work has been devoted to the development of some basic notions which can be used in an S matrix theory for systems of hyperbolic conservation laws in more than one space dimension, see [2,3,4].

Let $\vec{A} = \dfrac{\partial \vec{F}}{\partial \vec{u}}$ be the Jacobian matrix of $\vec{F}$. Equation (1.1) is said to be hyperbolic in a domain $D \subseteq R^{n+1}$ if the $s \times s$ matrix $\vec{A} \cdot \xi$ has real eigenvalues $\lambda_1, \ldots, \lambda_s$ for all $(\mathbf{x}, t) \in D$ and for all vectors ξ. If the eigenvalues λ_i are all distinct, the equation is said to be strictly hyperbolic. In the discussion which follows, hyperbolicity is assumed.

An S matrix theory is concerned with the large time asymptotic behavior of solutions to systems of equations for which system (1.1) is a first approximation. The leading order terms of these large time solutions are governed by the infinite scaling limit of the original system of equations. This scaling generally eliminates the higher order effects, yielding the

system (1.1). It is assumed that any source terms in the original equation are of bounded extend. Under scaling these source terms will in general survive and go into a multiple of a delta function at the origin.

An S matrix is the product of two wave operators, the outgoing operator W^+ which gives the large positive time asymptotics and the incoming wave operator W^- which gives the large negative time asymptotics. Attention will be focused on the outgoing wave operator W^+. The domain of W^+ usually taken to be the range of W^-. However, because of the occurrence of shocks in solutions of (1.1), this equation, when supplemented by the necessary entropy condition to separate physical from nonphysical waves, is not reversible. Thus W^- is not well defined. As a substitute the domain of W^+ will be restricted to scale invariant functions. Thus we consider solutions to the initial value problem for system (1.1) whose initial data is constant on rays through the origin. In some cases it will also be desirable to impose regularity conditions on the initial data as well. In one space dimension this is the well known Riemann problem and the problem of solving (1.1) with scale invariant data will be referred to as a multi-dimensional Riemann problem.

The notion of dimensionality in a Riemann problem is actually best described in terms of a co-dimension. A Riemann problem of co-dimension j is defined as the Cauchy problem for a system of conservation laws in d space dimensions in which the data is scale invariant in j dimensions and independent in the remaining $d - j$ dimensions.

The restriction to scale invariant data and the fact that equation (1.1) is itself scale invariant implies that a solution to a Riemann problem should be self-similar, that is, a function of $\frac{\vec{x}}{t}$. This implies that a Riemann solution $\mathbf{u}$ of (1.1) will satisfy

$$-\frac{\vec{x}}{t}\cdot\nabla\mathbf{u} + \nabla\cdot\vec{F} = 0. \tag{2.1}$$

Such a solution $\mathbf{u}$ is completely determined by its values in the hyperplane $t = 1$ and by restricting our attention to this hyperplane time can be eliminated from the equation. Therefore a Riemann solution of (1.1) has in general one less degree of freedom than a general solution.

General solutions for Riemann problems are known in a few special cases. If the number of space dimensions is one, the system is strictly hyperbolic and each eigenvalue is either genuinely non-linear or linearly degenerate, then the classical paper of Lax [5] describes the solution of a Riemann problem with a small discontinuity as consisting of shocks, centered rarefactions and contact discontinuities. If the equation is scalar and in two space dimensions, solutions are known in the case where $\vec{F}$ is of the form $f\vec{v}$, where f is a scalar valued function with at most one inflection point and $\vec{v}$ is a constant vector [6,7].

A central aspect of a scattering theory is that a source decomposes into some number of localized coherent waves, which then separate and propagate away from each other. These local disturbances are called $d-$dimensional elementary waves if the equation (1.1) is in d space dimensions. When d equals one these elementary waves include shocks, contact discontinuities and rarefaction waves. For $d>1$ elementary waves are defined by the interaction of lower dimensional waves, for example when two shocks or a shock and a contact discontinuity collide. In many cases, such as the interaction of two shock waves, these waves will move with a definite velocity. Assuming that the original equation (1.1) is invariant under Galilean boosts one can then make a translation to a reference frame in which the wave is at rest, thus eliminating one more degree of freedom from the equation.

Understanding the structure of these elementary waves is crucial in describing the solution of a Riemann problem. In some special cases this structure is known. As mentioned above, in the case of one space dimension, hyperbolicity and a suitable type of convexity for the flux function, a theory of Lax describes these elementary wave as consisting of shocks, contact discontinuities and rarefaction waves which correspond to the eigenvalues of the differential of the flux function. If the equation is scalar, then a general theory of Oleinik [8] describes these waves in terms of the convex envelope of the associated flux function. Other special cases in which the structure of elementary waves is known include one space dimension polytropic gas dynamics [9], two space dimension polytropic gas dynamics [10], adsorption with a Langmuir isotherm [11], and water and polymer displacement of oil without adsorption [12,13].

3. Two Dimensional Detonation Fronts

The method of front tracking has been applied to detonation waves in two-dimensional gas dynamics [14]. For problems which exhibit cylindrical symmetry comparisons can be made between the two-dimensional model and a one-dimensional model which exploits the symmetry and the agreement between these two methods is good. One finds that as the mesh of the computational grid is refined, the two-dimensional model converges linearly to the solution given by the model based on cylindrical symmetry.

Only a polytropic equation of state is considered, so the energy term E in (1.2) becomes:

$$E = \frac{p}{\gamma - 1} + \rho q + \frac{|\mathbf{m}|^2}{2\rho}.$$

Here q is the the energy released by the chemical reaction that occurs across the detonation front. The Chapman-Jouguet model of detonation is used. In this model it is assumed that the reaction takes place instantaneously and that the reaction zone is infinitely thin.

If state 0 is the unburned gas and state 1 is the burned gas, the states on the two sides of the detonation are related by:

$$M^2 = \frac{p_1 - p_0}{\tau_0 - \tau_1}, \tag{3.1a}$$

where M is the mass flux across the front, and the Hugoniot relation:

$$\frac{\gamma_0 \tau_0 p_0}{\gamma_0 - 1} - \frac{\gamma_1 \tau_1 p_1}{\gamma_1 - 1} - (q_1 - q_0) = \frac{(p_0 - p_1)(\tau_0 - \tau_1)}{2}. \tag{3.1b}$$

In the case of a Chapman-Jouguet (CJ) detonation, the detonation wave moves at the local sound speed with respect to the gas behind it [15], and the behind state is completely determined by the ahead state and equations (3.1). When the combustion front is a strong detonation one additional parameter is necessary in order to specify the behind state from the ahead state.

A series of both strong and CJ detonation runs using grid sizes of 5 by 5, 10 by 10, 20 by 20, 40 by 40 and 80 by 80 have been made. The contact discontinuity behind the detonation front and the detonation front itself were tracked. Several of these runs were initially cylindrically symmetric and in these cases comparisons were made with a one-dimensional computation using the random choice method with 1500 points in the radial direction.

Figs. 3.1 - 3.5 present the results of a cylindrically symmetric computation in which the initial pressure ratio across the front is 100. The initial density is uniform and the gas releases 92.65% of its internal energy upon combustion. Figs. 3.1 and 3.2 show the positions of the contact (inner quarter circle) and the detonation (outer quarter circle) at the beginning and end of the run respectively. Other figures include comparisons of pressure profiles and detonation wave speed (see Figs 3.3 and 3.4). The detonation wave speed error when calculated with respect to the one-dimensional code is less than 0.5%. Fig. 3.5 shows the convergence of the front tracking code to the one-dimensional code under mesh refinement.

In addition to cylindrically symmetric runs the front tracking code has also been applied to problems in which the initial interface is elliptical. If the initial states are the same as the ones described above, hot spots are produced behind the front in regions of small curvature and cold spots in corresponding regions of large curvature. The initial lengths of the major and minor axes are .3 and .15 for the detonation wave and .29 and .145 for the contact. Fig. 3.6 shows pressure contours and the waves just before the detonation wave breaks through the boundary on a 30 by 30 grid. The pressure is higher behind the flatter portion of the detonation wave than behind the rounder portion of the wave.

4. Supersonic Interface Instabilities

Interface fingering instabilities arise in a wide variety of physical contexts: inertial laser fusion, plasma fusion, instabilities of layers in stars, the instability of laser accelerated foils, and astrophysical jets. We have examined the compressible Rayleigh-Taylor instability of a supersonic accelerated contact discontinuity between two gases. The computed solutions

exhibit a complicated set of nonlinear waves comprised of spike and bubble bow shocks, terminal shocks within the spike and bubble, Kelvin-Helmholtz roll-up of the spike tip, and contact surface waves. Detailed analysis is given in Ref. [16]. We have also studied the propagation of a supersonic slab jet in order to compare and contrast the jet wave structure with that of the supersonic accelerated surface.

A compressible gas interface which is accelerated by a shock (the Meshkov-Richtmyer instability [17,18]) is Rayleigh-Taylor unstable. If the interface is accelerated by a gravitational field, then the interface is unstable when the light fluid pushes the heavy. The important features of this instability can be modeled by imparting an initial kinetic energy to the contact discontinuity, which subsequently is allowed to advect freely. We assume that the problem is periodic in x with reflecting boundaries at the top and bottom of the computational region.

The problem can be parametrized in dimensionless units by the initial Mach number of the tip of the spike with respect to the heavy gas and by the initial density ratio ρ_b/ρ_a (b denotes the gas below the contact, a the gas above). The dimensional scales are set by the initial ambient pressure, perturbation wavelength, and initial ambient density of the heavy gas. The polytropic gas constant γ was set equal to 1.4.

An interesting set of wave structures emerges from this study. Figure 4.1 portrays the evolution of a Mach 2.8 density ratio 2 accelerated surface at $t = 0.4$. The flow is initially supersonic in both gases. The bow shocks in the lower gas have interacted to form a single shock, while the spike bow shock has interacted and joined with its periodic neighbors. The spike exhibits the characteristic Rayleigh-Taylor roll-up, and the contact shape indicates the presence of small-scale surface instabilities.

Just inside of the advancing spike a "terminal" shock wave is formed. The contact is advancing more slowly than the heavy gas inside of the spike. A shock wave, preceded by a rarefaction wave, is formed as the advancing heavy gas is slowed down to the contact velocity. A similar terminal wave is formed in the light gas inside of the advancing bubble.

This shock preceded by a rarefaction wave pattern can be clearly seen in the density cross section plots in both the supersonic accelerated surface run (Figure 4.1) and the

supersonic jet run (Figure 4.2). Note that while the jet terminal shock propagates with the head of the jet beam, the accelerated surface terminal shocks are physical transients which decouple from the late evolution of the contact instability.

The compressible Rayleigh-Taylor results differ from the incompressible case chiefly in the formation of the terminal compression waves and in the fact that the spike exhibits less roll-up. The accelerated surface problem differs from the gravitational instability in that the spike appears to attain a finite growth of aspect ratio approximately equal to 2 for our range of parameters.

A resurgence of interest in supersonic jets has been sparked by the observation of astrophysical jets emanating from the cores of active galaxies and by the subsequent success of theoretical [19] and computational analyses [20].

The evolution of a Mach 3, density ratio 10 slab jet at $t = 0.4$ is presented in Figure 4.2 [16]. The jet was initialized by injecting gas at a specified Mach number into an ambient gas at equal pressure. The boundary conditions are through-flow. The problem is parametrized by the Mach number of the jet with respect to the jet gas and the density ratio of jet to ambient gas. γ was set equal to 5/3. The results apply to jets from laboratory to astrophysical scales since the problem is independent of length scale.

The jet beam in our 80x120 grid computation is 5 grid blocks wide, while the beam is 20 grid blocks wide in the 160x300 grid computation of Norman, Smarr, and Winkler [20].

The density contour and cross-section plots in Fig. 4.2 indicate the presence of a bow wave (the flow is subsonic in the ambient gas) and of a terminal shock near the head of the jet beam, preceded by a rarefaction wave. This terminal shock system may explain the observed hot spots terminating astrophysical jets [20]. The contact shape displays the large scale Kelvin-Helmholtz roll-up of this jet, and the development of two-dimensional pinch waves.

The fact that we get reasonable results with a beam 5 grid blocks across illustrates one of the advantages of the front-tracking method. By placing additional degrees of freedom around the tracked contact, the method is able to resolve the solution globally with fewer degrees of freedom than required by conventional finite difference methods. The importance

of this feature of the method will become apparent when the statistical regime of multiple fingers is considered.

5. Numerical Implementation of Elementary Waves

Further work on the development of computer code for modeling elementary waves is in progress. Previous papers [10,1] have reported the numerical implementation in the front tracking code of the elementary waves known as regular reflection and single Mach reflection, this section will discuss the case of shock and contact discontinuity interactions.

The simplest model of a shock and contact discontinuity interaction consists of an incident shock wave colliding with a contact discontinuity separating two different gases. The local result of this interaction is a configuration we call a diffraction node. A diffraction node consists of the incident shock wave, the contact discontinuity into which the incident shock collides, a reflected wave which is either a shock or a centered rarefaction wave and a deflected contact surface behind the incident shock. The model supposes that locally all of the shock or contact waves can be assumed to be straight, and that the solution in a neighborhood of the node is piecewise constant except for the possible reflected centered rarefaction wave. It is assumed that the point of intersection of these waves moves with a definite velocity and thus the interaction can be studied in a frame of reference in which the node is at rest. The description of a diffraction node then consists of the states in a neighborhood of the node together with the angles at which the waves at the node intersect.

In a dynamic model it is necessary to calculate the transformation to the steady frame of the node. This is equivalent to finding the velocity of the node in the given reference frame. This velocity can be approximated by propagating the incident shock and the contact discontinuity into which it collides for one time step ignoring their interaction. The intersection of the two propagated curves is then used as the updated node position from which the node velocity can be calculated. Once the node velocity is known, the transformation to the steady frame of the node is performed. If one assumes that the data in front of the incident shock on both sides the contact discontinuity is known, and the strength of the incident shock is

given, then the configuration around the diffraction node in the steady frame can be found by the intersection of shock polars in the pressure turning angle space, see Henderson [21]. Finally the configuration is translated back to the original frame of reference.

Figure 5.1 shows the result of the interaction of a planar shock wave colliding with a sinusoidally perturbed contact discontinuity. The incident shock is in air ($\gamma = 1.402$) and the contact surface separates air from sulphur hexafluoride ($\gamma = 1.092$). This interaction is known as a fast-slow interaction since the sound speed in air is greater than that in sulphur hexafluoride. The initial shock has a pressure behind to pressure ahead ratio of 100. It is interesting to note the extreme proximity of the transmitted shock and the deflected contact discontinuity near the node. We were quite pleased with the front tracking code's ability to resolve a configuration with such close curves. The rectangular mesh used for this run was 20x20, and the separation between the transmitted shock and deflected contact is on the order of one tenth of a mesh block for a large portion of the computational region. Furthermore the transmitted wave lies on the sulphur hexaflouride side of the contact discontinuity and the value of gamma for this gas is so close to one as to make the resolution of waves on moderate sized grids difficult for most finite difference methods. We suspect that without front tracking one would need a rectangular mesh more than ten times as fine in each linear dimension in order to resolve both the deflected contact and the transmitted wave.

6. Bifurcations and Wave Interactions

One of the principal difficulties in any front tracking code is the handling of bifurcations and interactions in the tracked interface. Examples of these include the transition from regular to Mach reflection and the passing of waves through computational boundaries. Interactions of both of these types have been either fully or partially implemented in our front tracking code.

Figure 6.1 shows a planar shock wave incident upon a ramp. The problem is initialized with the shock normal to the wall. When the ramp is reached, a bifurcation occurs, in this

case to a regular reflection. At a later time the point of regular reflection reaches the top of the ramp. At this point the regular reflection node lifts off the wall producing a Mach type reflection.

In figures 6.2 the front tracking code is used to follow the development of a compressible Kelvin-Helmholtz roll-up [1,22]. Initially two gases of equal pressure and temperature but moving in opposite directions are separated by a slip discontinuity. This slip surface is given an initial perturbation which causes it to roll-up. The boundary conditions at the sides of the computational rectangle are periodic. As the surface rolls up portions of the surface cross the periodic boundaries. Any section of the surface which propagates past a periodic boundary is disconnected from the original curve and reinstalled periodically shifted to the opposite side of computational rectangle. A linking between the periodically connected curves is maintained so that periodic boundary conditions are enforced. The visual effect is that as one section of the slip surface propagates out of the computational window, we see the corresponding portion of the periodic neighbor moving into our picture.

Not only is the interaction of curves with computational boundaries of interest, but the interaction of nodes as well. Fig. 6.3 shows a diffraction node propagating past a computationally passive boundary. This problem is supersonic and the signals from the exterior of the right hand boundary are sufficiently weak that their influence on the solution can be ignored. Thus the problem of node passing through such a boundary is simply a matter of identifying those curves at the exiting node which leave and those which remain. Exiting curves are deleted and the remaining curves are separately installed on the boundary. The main difficulty here is dealing with the numerical degeneracies which occur because very short curves are produced when the node first crosses the boundary.

References

1. I-L. Chern, J. Glimm, O. McBryan, B. Plohr, and S. Yaniv, "Front Tracking for Gas Dynamics," *J. Comp. Phys.*, vol. To appear.

2. James Glimm, "Elementary Waves and Riemann Solutions. Their Theory and Their Role in Science," *DOE Research and Development Report DOE/ER/03077-249*, 1985.

3. James Glimm and D. H. Sharp, "Elementary Waves for Hyperbolic Equations in Higher Space Dimensions: An Example from Petroleum Reservoir Modeling," *DOE Research and Development Report DOE/ER/03077-248*, 1985.

4. James Glimm and D. H. Sharp, "An S Matrix Theory for Classical Nonliner Physics," *Foud. of Physics*, vol. To appear.

5. P. Lax, "Hyperbolic Systems of Conservation Laws II," *Comm. Pure and Appl. Math*, vol. 10, pp. 537-566, 1957.

6. W. B. Lindquist, "Construction of Solutions for Two Dimensional Riemann Problems," *Adv. Hyp. PDE's.*, (To Appear).

7. W. B. Lindquist, "The Scalar Riemann Problem in Two Spatial Dimensions: Sufficiency Condition for Piecewise Smoothness of Solutions and its Breakdown," *J. Math. Anal.*, SIAM, (To Appear).

8. O. A. Oleinik, "Discontinuous Solutions of Non-Linear Differential Equations," *Uspehi Mat. Nauk*, vol. 12, pp. 3-73 (1957). English transl., Amer. Math. Soc. Transl. Ser. 2, vol. 26 (1963), 95-172

9. J. Smoller, *Shock Waves and Reaction-Diffusion Equations*, Springer Verlag, New York, 1983.

10. J. Glimm, C. Klingenberg, O. McBryan, B. Plohr, D. Sharp, and S. Yaniv, "Front Tracking and Two Dimensional Riemann Problems," *Adv. in Appl. Math.*, vol. To appear.

11. F. Helfferidge and G. Klein, *Multicomponent Chromatography: Theory of Interference*, Marcel Dekker, New York, 1970.

12. B. Keyfitz and H. Kranser, *J. Diff. Eqs.*, vol. 27, p. 444, 1978.

13. E. Isaacson, *J. Comp. Phys.*, vol. To appear.

14. B. Bukiet, "Application of Front Tracking to Two Dimensional Curved Detonation Fronts," *To appear*.

15. R. Courant and K. O. Friedrichs, *Supersonic Flow and Shock Waves*, p. 212, Springer Verlag, New York, 1948.

16. C. L. Gardner, "Compressible Rayleigh-Taylor Instability of Supersonic Accelerated Surfaces," *To appear.*

17. R. D. Richtmyer, "Taylor Instability in Shock Acceleration of Compressible Fluids," *Comm. Pure and Appl. Math*, vol. 13, p. 297, 1960.

18. E. E. Meshkov, *Izv. Akad. Nauk SSSR, Mekh. Zhidk. Gaz.*, vol. 5, p. 151, 1969.

19. R. D. Blanford and M. Rees, *Mon. Roy. Astr. Soc.*, vol. 169, p. 395, 1974.

20. L. L. Smarr, M. L. Norman, and K-H.A Winkler, *Physica*, vol. 12D, p. 83, 1984.

21. L. F. Henderson , "The Refraction of a Plane Shock Wave at a Gas Interface," *J. Fluid Mech.* , vol. 26, p. 607, 1966 .

22. B. Plohr, J. Glimm, and O. McBryan, "Applications of Front Tracking to Two-Dimensional Gas Dynamics Calculations," in *Lecture Notes in Engineering Vol. 3*, ed. J. Chandra and J. Flaherty, p. 180, Springer Verlag, New York, 1983.

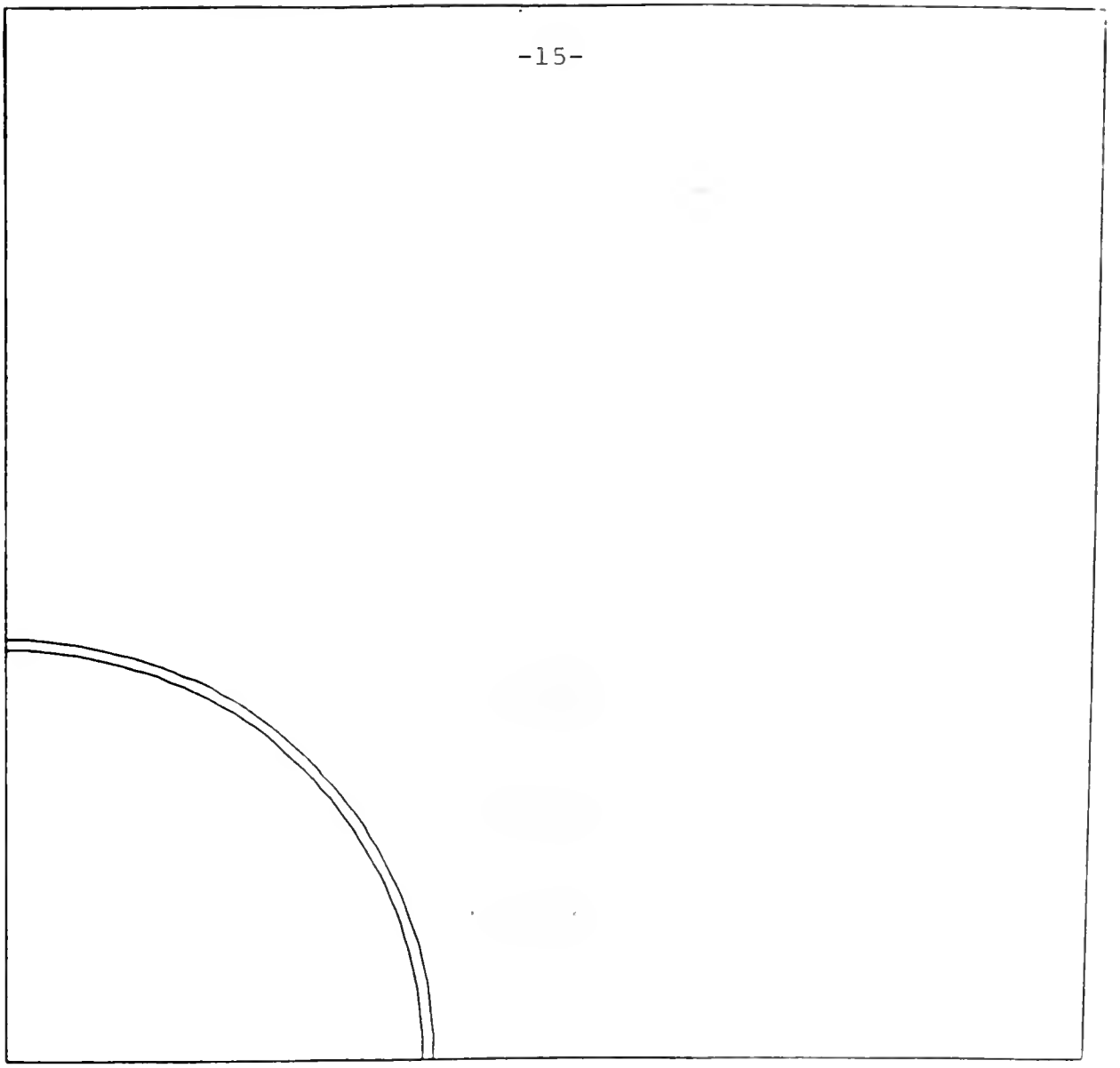

Fig. 3.1
The initial strong detonation wave (outer circle) and the contact discontinuity for a cylindrically symmetric computation. The initial conditions are uniform density, zero velocity, and a circular pressure discontinuity at radius .2, with ratio inside to outside of 100. The heat released upon combustion is 92.65% of the internal energy of the unburned gas. The initial position of the contact is radius .195. The initial state between the waves is that behind a planar detonation wave with the above initial data.

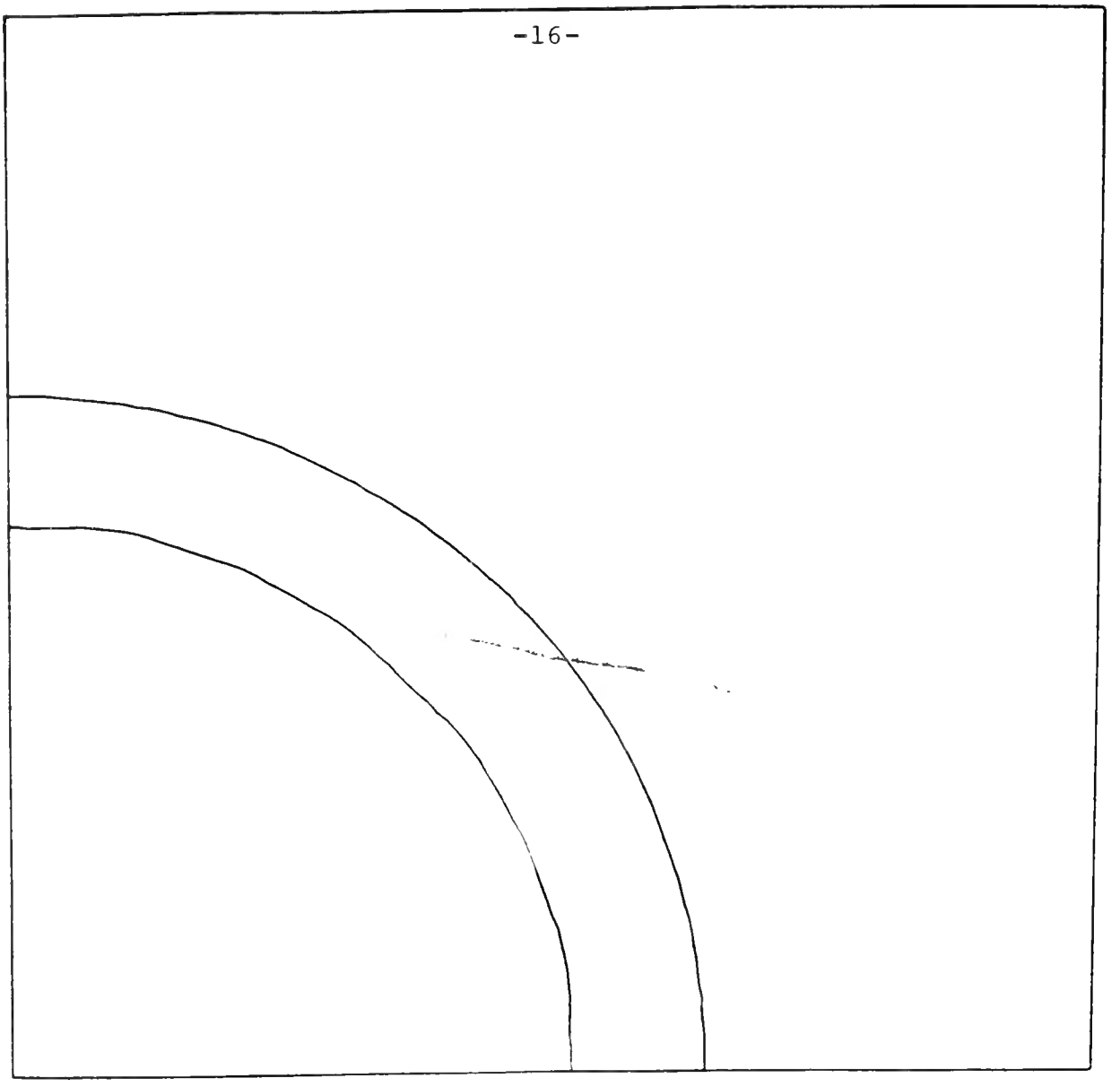

Fig. 3.2
The detonation wave and the contact at the time step analyzed in Figs. 3.3 and 3.4. The detonation wave now has radius approximately .36.

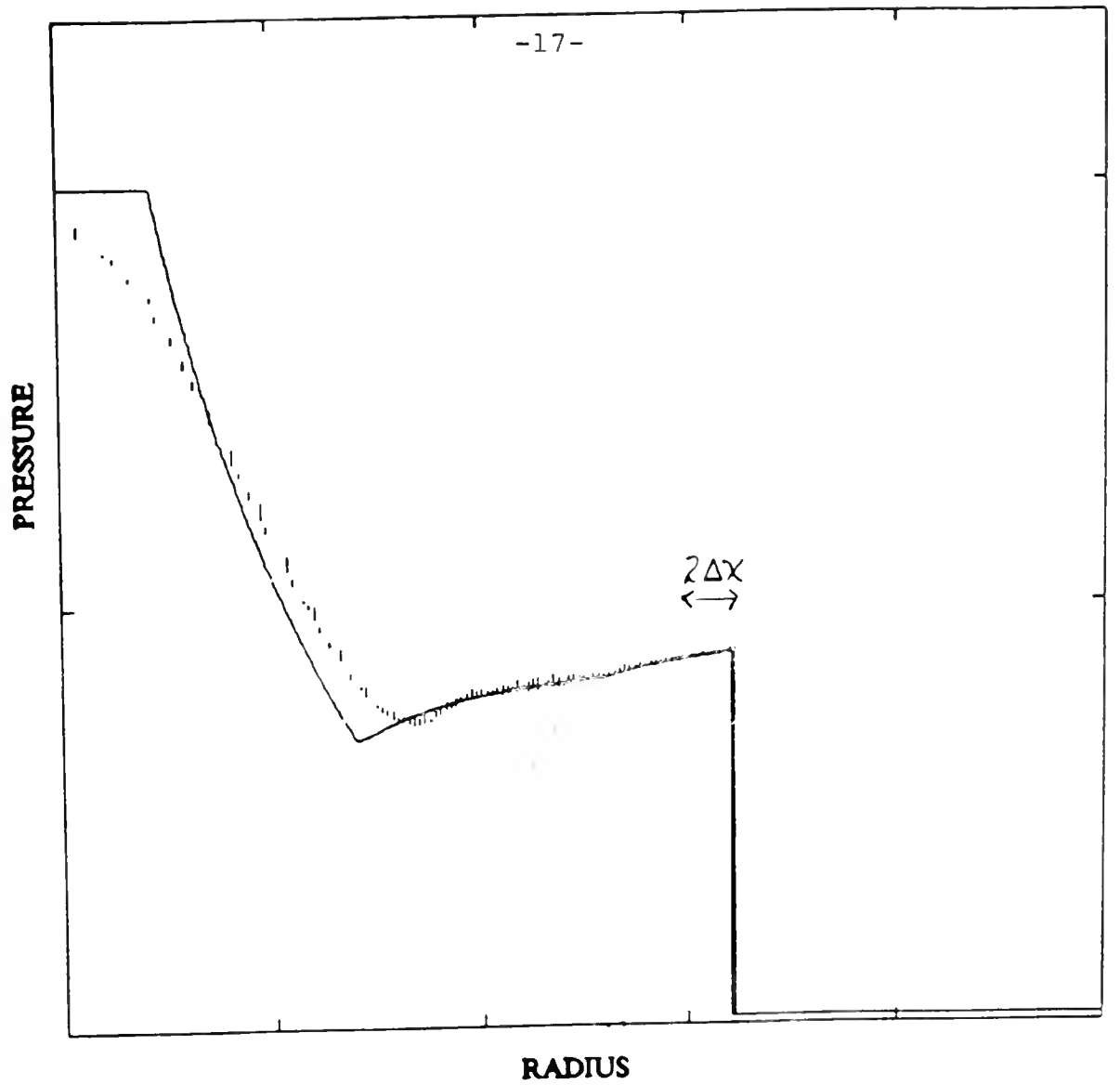

Fig. 3.3
A plot of presure vs. radius corresponding to Fig. 3.2 is shown. The solid curve shows the results obtained by the one-dimensional random choice computation. The vertical lined represent the range of pressure values in the two-dimensional front tracking solution at a fixed radius as the angle varies on a 40 by 40 grid. Thus, the vertical lines show the angular dependence in the solution.

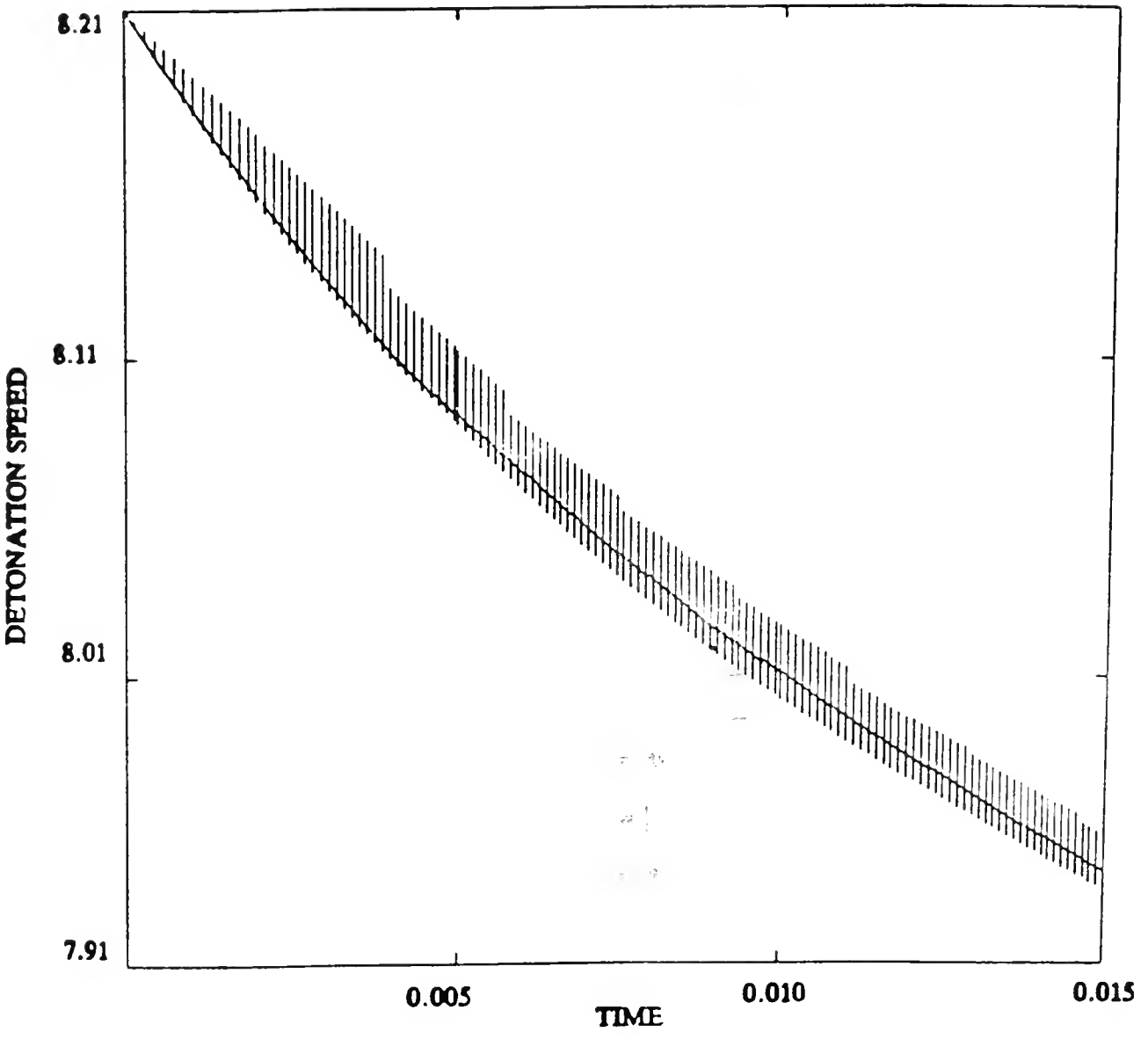

Fig. 3.4

A plot of detonation speed vs. time for the computation on a 40 by 40 grid. The solid curve shows the speed of the detonation wave in the one-dimensional calculation. The vertical lines represent the range of values of the speed of the detonation in the two-dimensional calculation. The maximum error ($\max \frac{|U_{2d} - U_{1d}|}{U_{1d}}$) is less than 0.5%.

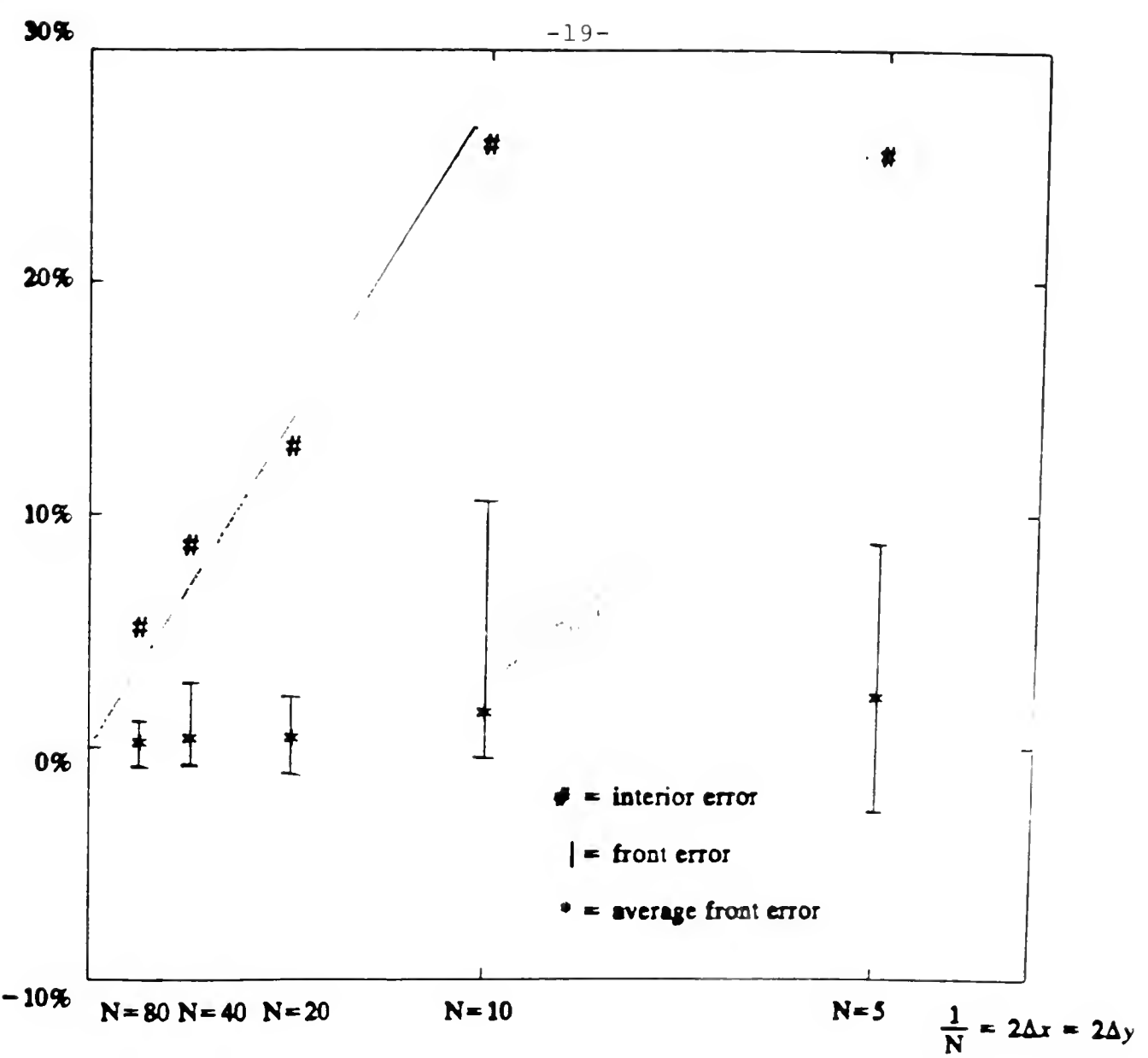

Fig. 3.5
Convergence of the front and interior schemes. The pressure errors in the interior and at the front are shown for NxN grids at the time indicated by Fig. 3.2. The # signs represent the interior error, where

$$\text{Interior Error} = 100\% \times \frac{\int_0^5 \int_0^5 |P_{2d} - P_{1d}| dxdy}{\int_0^5 \int_0^5 P_{\text{initial data}} dxdy}$$

The front error (error bars) gives the range of the errors at the front, defined as

$$\text{Front Error} = 100\% \times \frac{P_{2d} - P_{1d}}{[P]},$$

where [P] is the pressure jump at the front in the one-dimensional computation at the same time. The asterisks represent the error of the average pressure behind the front, namely

$$\text{Front Error(average pressure)} = 100\% \times \frac{P_{2d\ average} - P_{1d}}{[P]}.$$

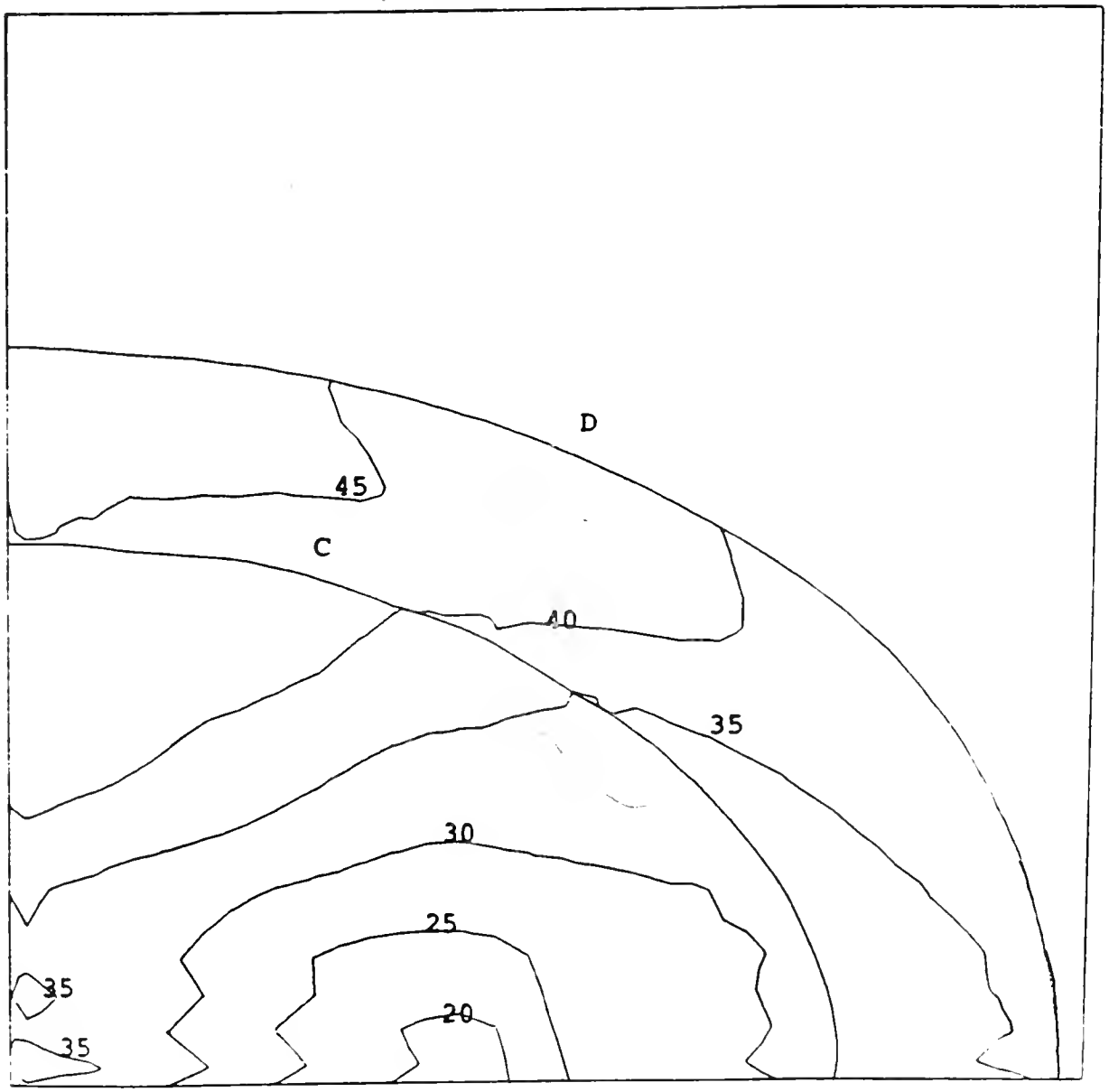

Fig. 3.6
Pressure contours are shown for a computation of an elliptical expanding detonation on a 30 by 30 grid. Also shown are the detonation wave (D) and the contact (C).

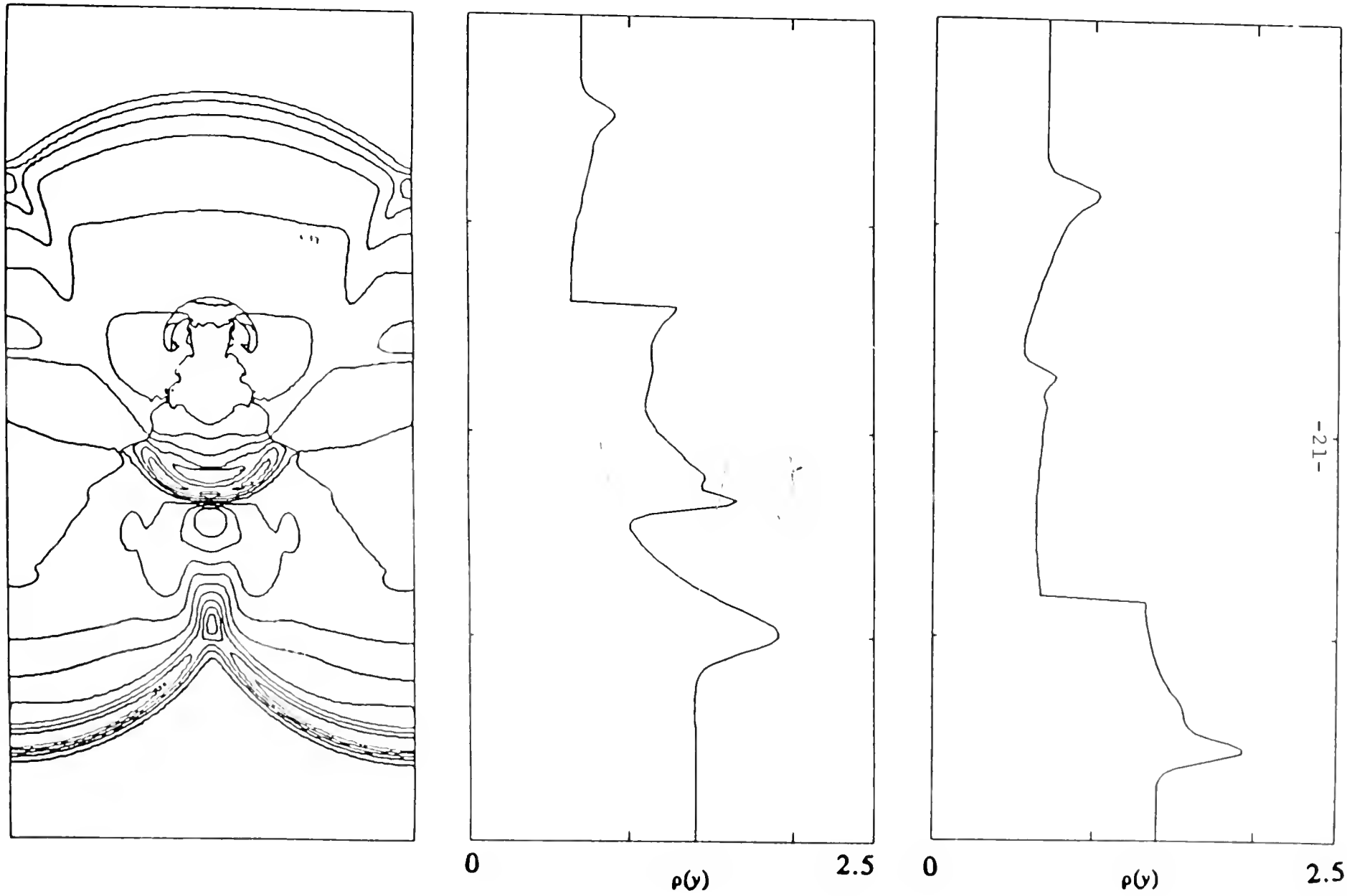

Fig. 4.1
M = 2.8, D = 2 density contours and density cross sections at t = 0.4. 80x160 grid.

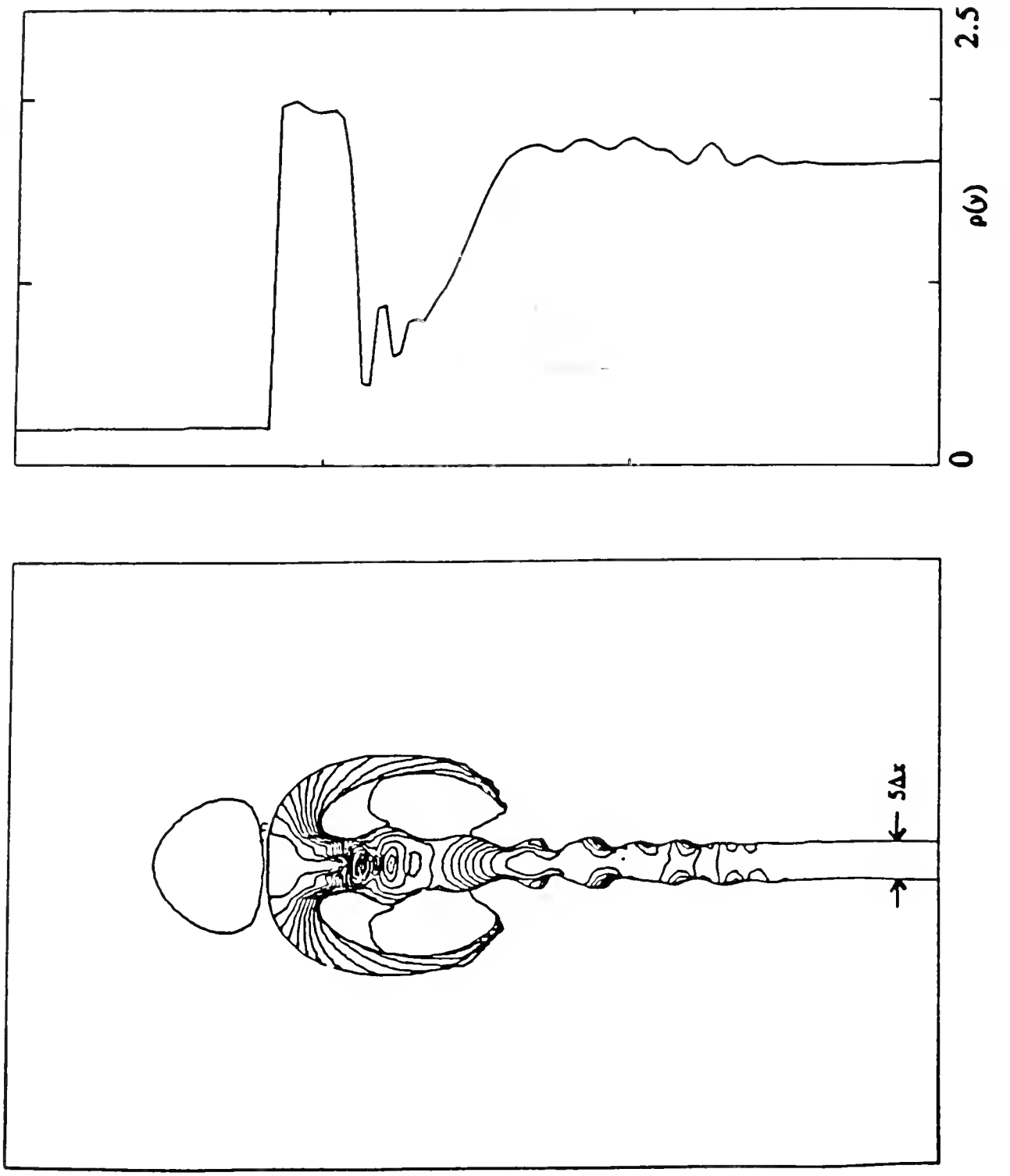
center-line density
2.5
0
ρ(y)
5Δx

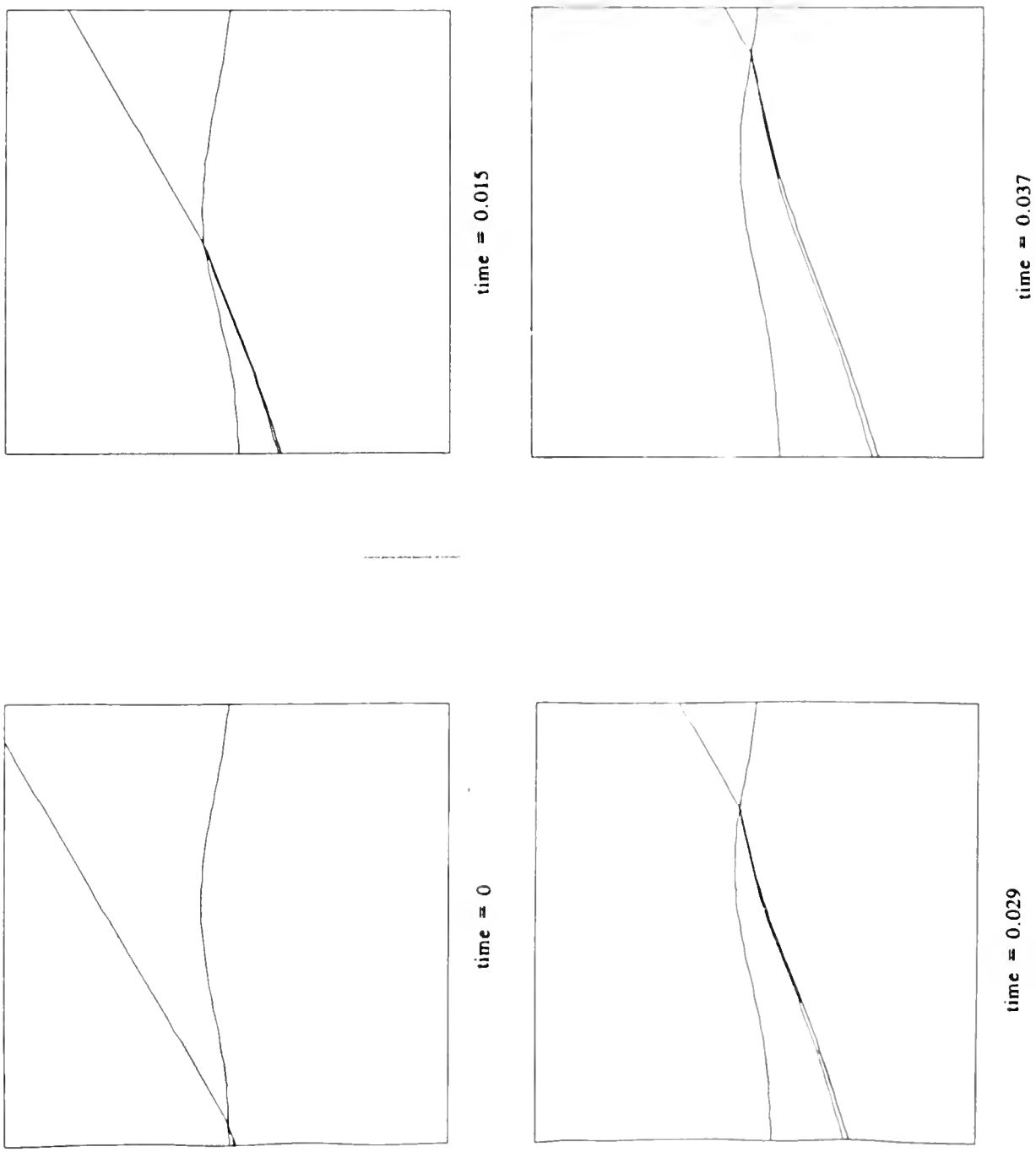

Fig. 5.1
The interaction of a shock wave with a contact discontinuity producing reflected and transmitted shock on a 20 by 20 rectangular grid.

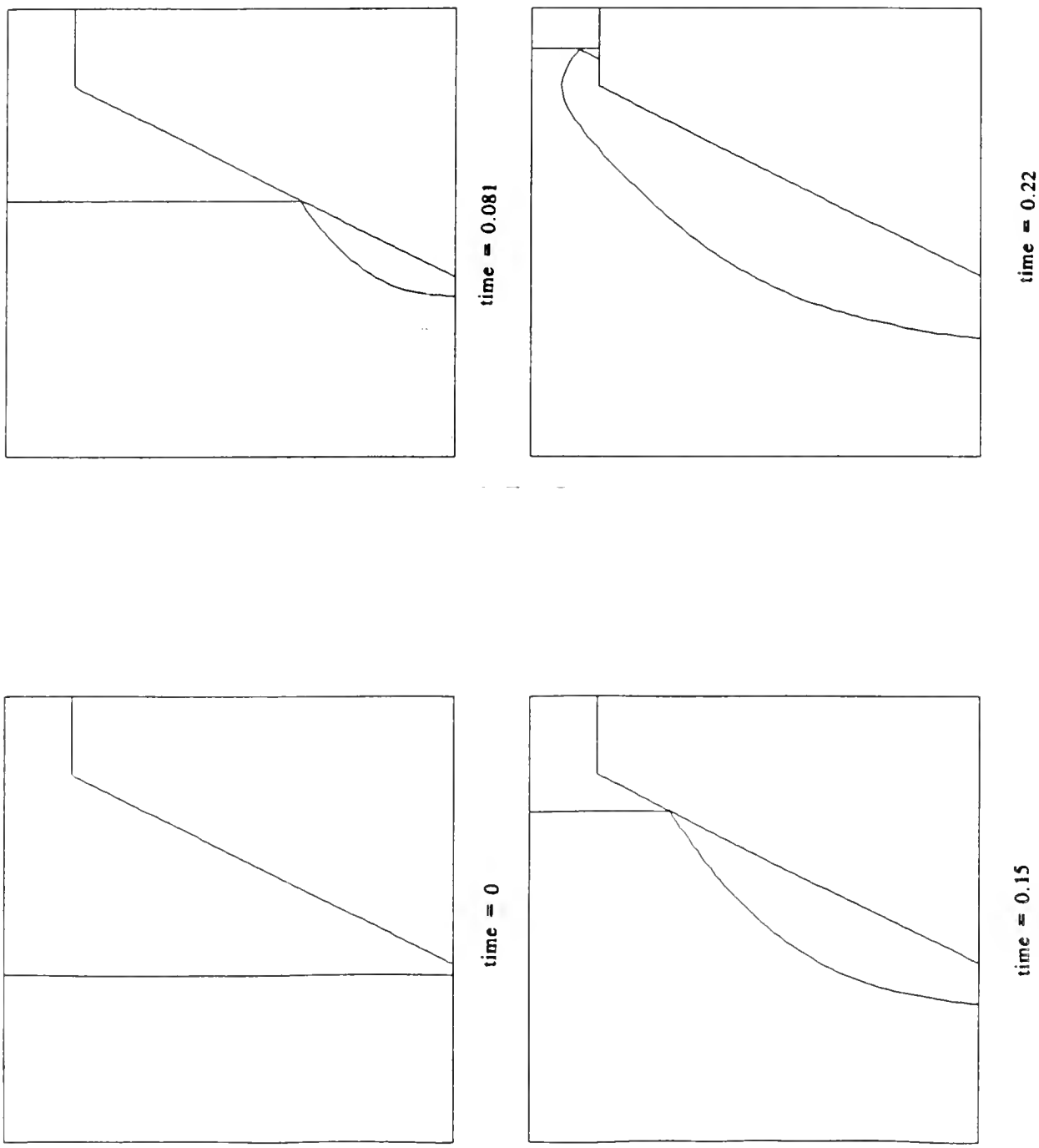

Fig. 6.1
A shock incident upon a ramp. Bifurcation to a regular reflection occurs when the shock reaches the ramp. When the regular reflection node reaches the top of the ramp a bifurcation to a Mach type reflection occurs. The grid here is 30 by 30.

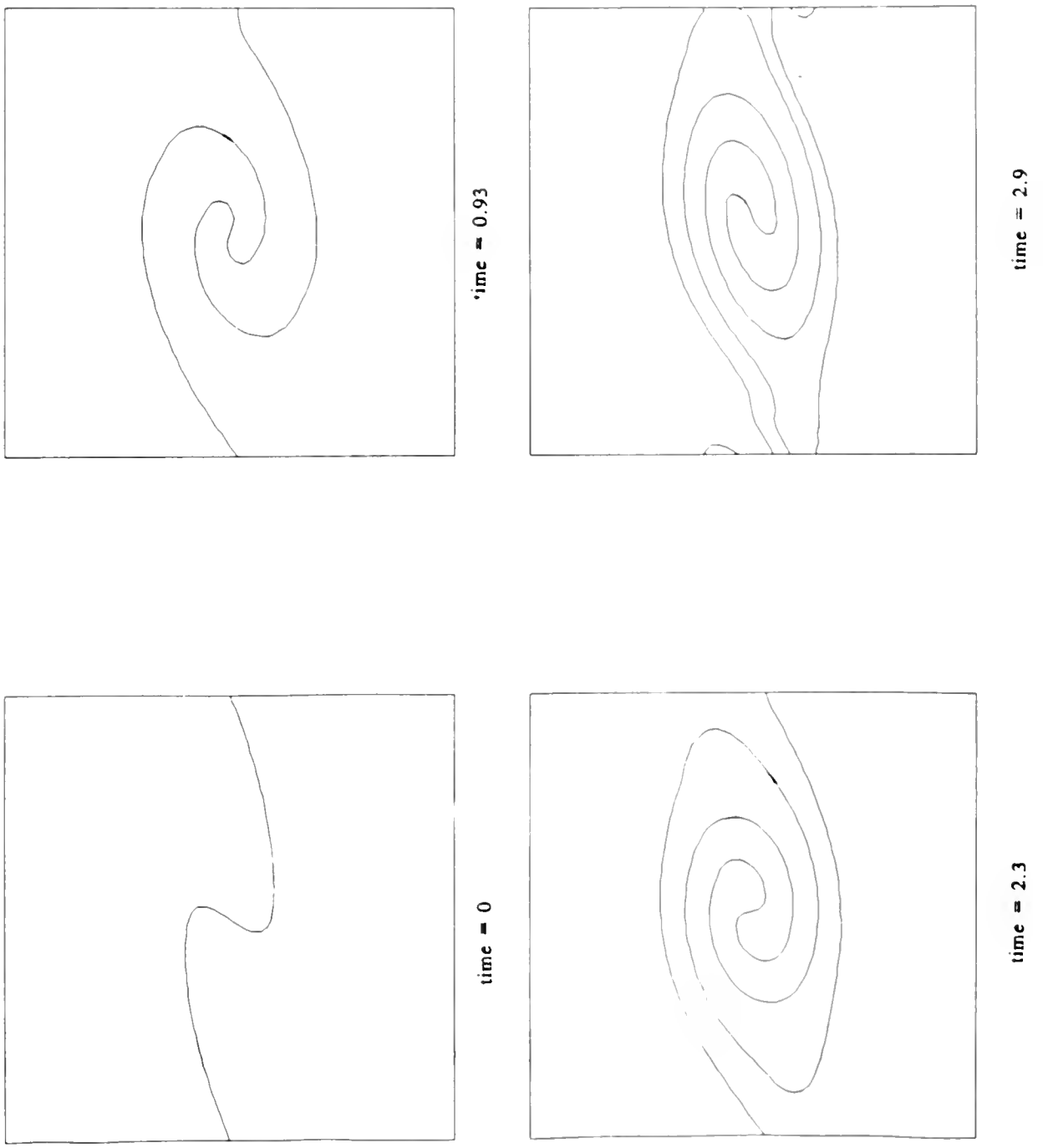

Fig. 6.2
Compressible Kelvin-Helmholtz roll-up. The computation is on a 40 by 40 grid. When interior curves cross the periodic boundaries at the side of the square, they are periodically reinserted on the opposite boundary.

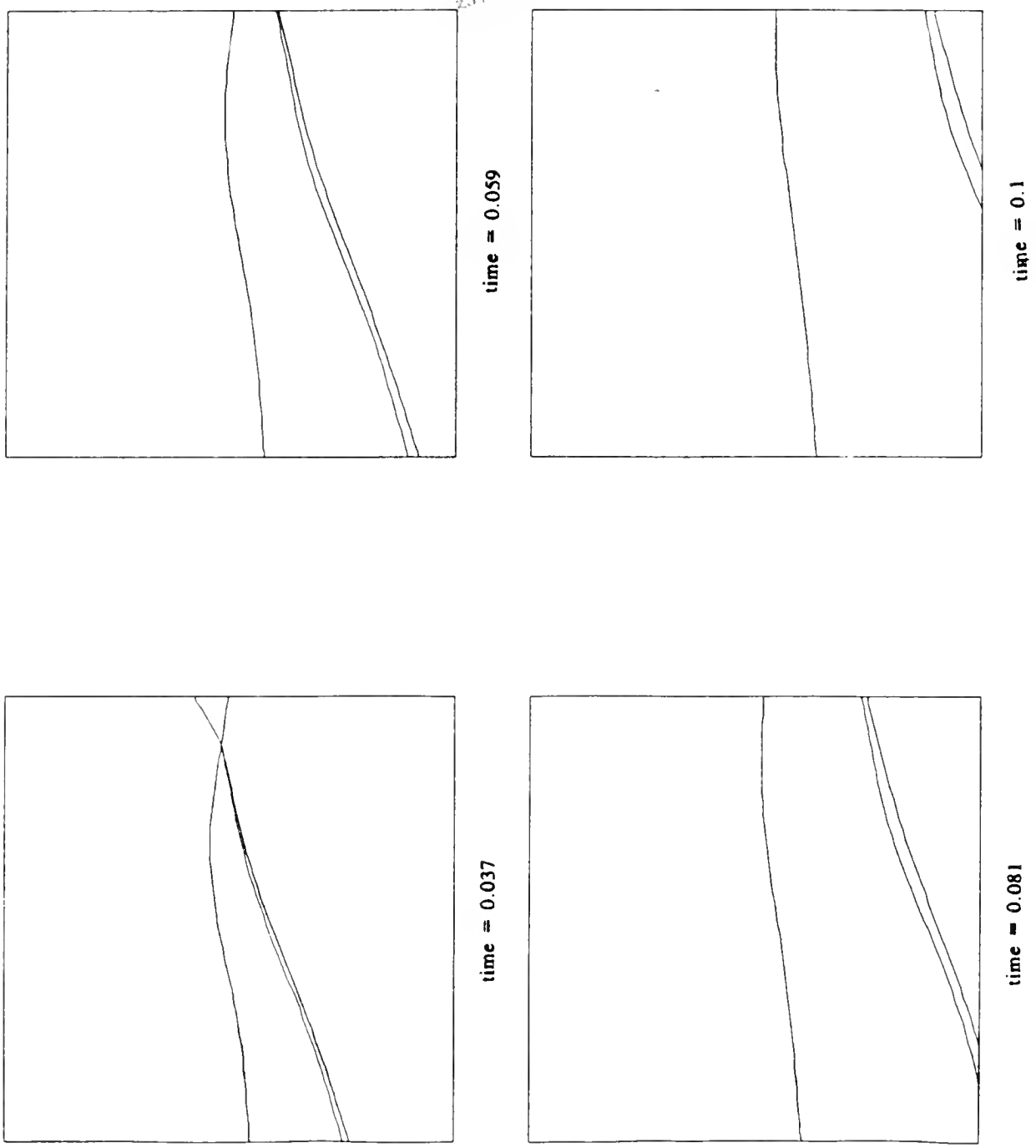

Fig. 6.3
Propagation of an interior node past a computationally passive boundary on a 20 by 20 grid. Signals from the outside of the computational domain are assumed to be negligible.

NYU DOE/ER/03077-266 c.1
Bukiet
Applications of front
tracking to combustion...